Atmos. Chem. Phys. Discuss., 11, 13911–13946, 2011
www.atmos-chem-phys-discuss.net/11/13911/2011/
doi:10.5194/acpd-11-13911-2011

Atmospheric Chemistry and Physics Discussions

Examination of aerosol distributions and radiative effects over the Bay of Bengal and the Arabian Sea region during ICARB using satellite data and a general circulation model

R. Cherian[1,2], C. Venkataraman[1], S. Ramachandran[3], J. Quaas[2,*], and S. Kedia[3]

[1]Department of Chemical Engineering, Indian Institute of Technology Bombay, Powai, Mumbai, 400 076, India
[2]Max Planck Institute for Meteorology, Hamburg, Germany
[3]Physical Research Laboratory, Ahmedabad, 380 009, India
[*]now at: University of Leipzig, Institute for Meteorology, Germany

Received: 30 December 2010 – Accepted: 1 May 2011 – Published: 6 May 2011

Correspondence to: R. Cherian (cherian.ribu@gmail.com)

Published by Copernicus Publications on behalf of the European Geosciences Union.

Abstract

In this paper we analyse aerosol loading and its direct radiative effects over the Bay of Bengal (BoB) and Arabian Sea (AS) regions for the Integrated Campaign on Aerosols, gases and Radiation Budget (ICARB) undertaken during 2006, using satellite data from the MODerate Resolution Imaging Spectroradiometer (MODIS) on board the Terra and Aqua satellites, the Aerosol Index from the Ozone Monitoring Instrument (OMI) on board the Aura satellite, and the European-Community Hamburg (ECHAM5.5) general circulation model extended by Hamburg Aerosol Module (HAM). By statistical comparison with large-scale satellite data sets, we firstly show that the ship-based ICARB observations are representative for the entire northern Indian Ocean during the pre-monsoon season. In a second step, the modelled aerosol distributions were evaluated by a comparison with the measurements from the ship-based sunphotometer, and the satellites. It was found that the model reproduces the observed spatial and temporal variability in aerosol optical depth (AOD) and simulated AODs to a large extent. However, AOD was systematically underestimated during high-pollution episodes, especially in the BoB leg. We show that this underprediction of AOD is mostly due to deficiencies in the coarse mode, where the model showed that dust was the dominant component. The analysis of simulated dust AOD along with the OMI Aerosol Index showed that the too low dust emissions from the Thar Desert in the model are the main cause for this deficiency. Thirdly, we analysed the spatio-temporal variability of AOD comparing the ship-based observations to the large-scale satellite observations and simulations. It was found that most of the variability along the track was due to geographical patterns, with minor influence by single events. Aerosol fields were homogeneous enough to yield a good statistical agreement between satellite data at a 1° spatial, but only twice-daily temporal resolution, and the ship-based sunphotometer data at a much finer spatial, but daily-average temporal resolution. Finally, we estimated the shortwave aerosol radiative forcing. We found that the cruise represents well the regional-seasonal mean forcings. Constraining simulated forcings using the

ACPD
11, 13911–13946, 2011

Examination of aerosol distributions and radiative effects

R. Cherian et al.

observed AOD distributions yields a regional-seasonal mean aerosol forcing of −8.6, −21.4 and +12.9 $\mathrm{W\,m^{-2}}$ at the top of the atmosphere (TOA), at the surface (SUR) and in the atmosphere (ATM), respectively, for the BoB region, and over the AS, of, −6.8, −12.8, and +6 $\mathrm{W\,m^{-2}}$ at TOA, SUR, and ATM, respectively.

1 Introduction

Atmospheric aerosols play a significant role in regional and global climate by interacting with radiation (scattering and absorption) and modifying cloud microphysical properties, although the magnitudes of these impacts remain uncertain (Forster et al., 2007). Aerosols exhibit a large spatial and temporal variability, which impacts the spatial distribution of atmospheric heating (Ramanathan et al., 2001; Chung et al., 2005; Adhikary et al., 2007). Aerosol radiative effects have been linked to emission source categories with large uncertainties that resulted from the lack of knowledge about technologies used in various emission sectors (Reddy et al., 2005; Koch et al., 2007; Verma et al., 2008). In addition, the aerosol climate impacts are complex and difficult to quantify and to observe (Forster et al., 2007; Reddy et al., 2005). Therefore, investigations of aerosol distributions, along with an understanding of emission sources, on regional scales are needed to probe uncertainties in their atmospheric abundance and climate impacts.

Recent observational and modeling studies found large spatial and seasonal heterogeneities in aerosol chemical and physical properties over the Indian region (Reddy et al., 2004; Chung et al., 2005; Adhikary et al., 2007; Verma et al., 2008; Moorthy et al., 2008; Kedia and Ramachandran, 2008; Ramachandran and Cherian, 2008). During the pre-monsoon season, from March to May, the westerly wind flow brings dry and polluted continental air masses over the Indian ocean along with clear-sky and minimal rainfall conditions. This provides an ideal situation to analyse the aerosol distributions and radiative effects. Several intense field campaigns have been conducted to characterize the aerosol distributions and its radiative effects during the north east

(NE) or winter monsoon season of January–March (e.g., Ramanathan et al., 2001; Ramachandran and Jayaraman, 2002). A recent observational campaign, the Integrated Campaign for Aerosols, gases and Radiation Budget (ICARB), was conducted over the BoB and AS region during 18 March to 10 May 2006 (Moorthy et al., 2008; Kedia and Ramachandran, 2008; Moorthy et al., 2009; Kedia et al., 2010), termed the pre-monsoon season, which precedes the south west (SW) or summer monsoon. The presence of significant spatio-temporal variations in aerosol loading (Moorthy et al., 2008; Kedia and Ramachandran, 2008) resulted in large spatial heterogeneities in the aerosol forcing and atmospheric heating patterns during this campaign (Moorthy et al., 2009; Kedia et al., 2010). Therefore, an understanding of the causes of the distinct spatio-temporal patterns in aerosols and associated radiative forcing during the ICARB period is needed.

General circulation models (GCM) simulate the processes of emission, chemical and physical transformations, removal mechanisms, transport, and radiative impact of aerosols. The simulated aerosol properties and their climate effects exhibit large uncertainties (Textor et al., 2006; Forster et al., 2007) due to the often inadequate representation of aerosol-related processes in climate models and inaccuracies in aerosol emission estimates (Textor et al., 2006). The aerosol optical depth as simulated by large-scale models was found to be underestimated by a factor of 2 over the Indian region (Reddy et al., 2004; Verma et al., 2008) and by a factor of 1.4 over the Asian region (Adhikary et al., 2007; Kinne et al., 2006). With the large spatial and temporal variability in aerosol distributions, model comparison studies with in situ and satellite observations become a valuable tool for studying aerosol climate effects over the Indian region.

In this study, we examined whether ICARB observations are representative of impact over the entire northern Indian Ocean during the pre-monsoon season. The columnar aerosol distributions are estimated using the European Centre for Medium-Range Weather Forecasts (ECMWF)-Hamburg (ECHAM, version 5.5) GCM combined with the Hamburg Aerosol Model (HAM). The current version of the model includes as aerosol

ACPD
11, 13911–13946, 2011

species sulfate, black carbon (BC), organic carbon (OC), dust, and sea salt. The large-scale datasets from the ECHAM5.5-HAM model and the MODIS satellite data were used to assess the representativeness of the ICARB ship-based observations. An analysis of the model-simulated aerosol distributions in comparison to measurements was carried out in this study using the observations from ships and satellites during the ICARB period. The model-simulated fine and coarse mode AODs were compared to satellite retrievals (MODIS) and used to estimate the columnar aerosol type and size distributions. We also present a constrained estimate of the direct aerosol radiative forcing in the shortwave (SW) spectrum at the top of the atmosphere (TOA), at the surface (SUR) and in the atmosphere (ATM).

2 Model description

2.1 The aerosol-climate model ECHAM5.5-HAM

Atmospheric simulations were made in the ECHAM5.5 GCM (Roeckner, 2003) with a horizontal resolution of T63 (about $1.8^{\circ} \times 1.8^{\circ}$) and a vertical resolution of 31 levels (extended from the surface to 10 hPa) combined with the aerosol module HAM (Stier et al., 2005). The main components of HAM are the microphysical module M7 (Vignati et al., 2004), an emission module, a sulfate chemistry scheme (Feichter et al., 1996), a deposition module, and a radiative transfer module (Stier et al., 2006). The aerosol components considered in HAM are sulfate, BC, OC, sea salt and mineral dust (Stier et al., 2005). The microphysical module of HAM predicts the evolution of an ensemble of seven internally mixed lognormal aerosol modes. The modes were composed either of compounds with no or low solubility, henceforth denoted as insoluble mode, or by an internal mixture of insoluble and soluble compounds, henceforth denoted as soluble mode (Stier et al., 2005). The size ranges considered are below 0.005 µm dry particle number median radius (r) for the nucleation mode, r between 0.005 and 0.05 µm for the Aitken mode, r between 0.05 and 0.5 µm for the accumulation mode, and r above

ACPD
11, 13911–13946, 2011

0.5 µm for the coarse mode (Stier et al., 2005).

Aerosol optical properties (single scattering albedo, extinction cross section, and asymmetry factor) are precalculated explicitly from Mie theory (Toon and Ackerman, 1981) and archived in a look-up table for a wide range of aerosol size distributions and refractive indices (Stier et al., 2005), and for 24 solar spectral bands (ranging from 0.25 µm to 4 µm). At each time step of the simulation, the aerosol optical properties were extracted from the look-up table for each mode as a function of the Mie size parameter ($x = 2\pi r/\lambda$, where r is the number median radius of the lognormal mode and λ is the wavelength) and of the real and imaginary parts of the refractive index. For internally mixed particles, the refractive index was calculated as a volume-weighted average of the refractive indices of all components present in the mode, including aerosol water (Stier et al., 2005).

2.2 Estimation of radiative forcing and heating rate

In ECHAM5.5-HAM, the instantaneous short wave direct aerosol radiative forcing (DARF (ΔF), W m^{-2}) was computed as the difference in the clear-sky net radiative fluxes, with and without the radiative properties of the total aerosols (Stier et al., 2007). Adjustment of stratospheric temperatures can be neglected in the forcing calculations (Stier et al., 2007). The DARF at TOA and SUR was estimated as the change in the net (downward minus upward) flux with and without the presence of aerosols in the atmosphere as:

$$\Delta F_{\text{TOA,SUR}} = \Delta F_{\text{with aerosol TOA, SUR}} - \Delta F_{\text{without aerosol TOA, SUR}} \tag{1}$$

The DARF within the atmosphere (ΔF_{ATM}) was estimated as the difference between the radiative forcing at TOA and SUR as:

$$\Delta F_{\text{ATM}} = \Delta F_{\text{TOA}} - \Delta F_{\text{SUR}} \tag{2}$$

The ΔF_{ATM} indicates the amount of radiative flux (energy) absorbed by the aerosols. The heating rate (K day^{-1}) resulting from the radiative flux (energy), which is converted

ACPD
11, 13911–13946, 2011

into heat, was estimated following Liou, 1980:

$$\frac{\partial T}{\partial t} = \frac{g}{C_p}\frac{\Delta F_{\mathrm{ATM}}}{\Delta p} \qquad (3)$$

where $\partial T/\partial t$ is the heating rate (K day^{-1}), g is the acceleration due to gravity, C_p is the specific heat capacity of air at constant pressure, ΔF_{ATM} is the DARF within the atmosphere and p is the atmospheric pressure (Liou, 1980). In this study Δp is considered as 300 hPa which is approximately equal to the pressure difference over the planetary boundary layer height (between the surface and 4 km), in which the dominant part of atmospheric aerosol concentrations were found (e.g., Ramanathan et al., 2001; Forster et al., 2007; Kedia et al., 2010).

3 Data sets

3.1 ICARB cruise measurements

AOD measurements were made using a handheld sunphotometer instrument during the ICARB cruise expedition, conducted on the Oceanographic Research Vessel Sagar Kanya during 18 March to 10 May 2006 (Kedia and Ramachandran, 2008). The first phase of ICARB was conducted over the BoB during the period from 18 March to 12 April 2006 and the second phase of ICARB was conducted over the AS during the period from 18 April to 10 May 2006. About 40 observations were made each day at 15 min interval from 08:00 Local Standard Time (LST) to 17:00 LST in a moving frame over the ocean during clear sky conditions (Kedia and Ramachandran, 2008).

3.2 MODIS and OMI data

In this study, satellite observations were compared to the model outputs and to ICARB ship-based remote sensing. The daily Level 3 MODIS (collection V005) global 1°×1°

Discussion Paper | Discussion Paper | Discussion Paper | Discussion Paper |

ACPD

11, 13911–13946, 2011

Examination of aerosol distributions and radiative effects

R. Cherian et al.

gridded AOD and fine mode fraction (FMF) (Remer et al., 2005) values at 550 nm from both Terra and Aqua satellites were obtained during the ship cruise period for clear-sky pixels.Where less than 20 valid retrievals (optical depth pixel counts less than 20) were available in a 1°×1° grid-box (i.e., where cloudy skies are prevalent), AODs were weighted down (multiplied by a factor of 0.7) to avoid the potentially large influences of satellite retrieval errors such as cloud contamination, or domination by aerosol swelling in large relative humidities around clouds. When AOD values are aggregated to the 1°×1° grid, these discrepancies might otherwise be propagated into larger biases (Kahn et al., 2007). The daily Level 3 global 1°×1° gridded UV aerosol index (AI) from the Aura OMI sensor (http://gdata1.sci.gsfc.nasa.gov/daac-bin/G3/gui.cgi?instance_id=omi) were analysed during 18 March–10 May 2006 to study the dust source locations relevant to the BoB and AS regions. UV AI is the difference between the observed and model estimated absorbing and non absorbing spectral radiances at 360 and 331 nm (http://disc.sci.gsfc.nasa.gov/PIP/shtml/aerosol_index.shtml). AI is a particularly useful parameter for tracking regional transport of dust aerosols, which have strong absorption in the UV spectral region.

4 Simulation setup and approach

In this section we briefly report the aerosol emission inventory details and the experiments performed within this study. Aerosol emissions, based on the AEROCOM emission inventory (Dentener et al., 2006) of the year 2000, combined with regional emission inventories available over India (Reddy and Venkataraman, 2002; Venkataraman et al., 2005; Venkataraman et al., 2006) were used for biofuel, fossil fuel, industry and wild fire emission categories. SO_2 emissions include volcanoes (Andres and Kasgnoc, 1998), vegetation fires, industry, fossil fuel and biofuel (Cofala et al., 2005). In this study, fossil fuel emissions over the Indian region were projected from base year 1999 (Reddy and Venkataraman, 2002) to the year 2006 using International Energy Agency (IEA) fuel consumption data. Emissions from residential cooking with biofuels

ACPD
11, 13911–13946, 2011

(Venkataraman et al., 2005) were projected to 2006 using population data, while those from agricultural residue burning were directly used from Venkataraman et al. (2006). Except for DMS, 97.5 % of all sulfuric emissions are assumed to be in the form of SO_2 and 2.5 % in the form of primary sulfate particles following Dentener et al. (2006). The dust and sea salt emissions were calculated online (Tegen et al., 2002; Schulz et al., 2004) using the ECHAM5.5 10 m wind speed.

For the experiment, a model spin-up of three months was performed to initialize aerosol fields, and continued with a simulation of the March–May 2006 period for analysis. The large scale meteorology was constrained by nudging the model winds to 6-hourly ECMWF analysis meteorological fields (Simmons and Gibson, 2000). The nudged simulations allow for a fair comparison of modeled parameters with the field campaign measurements.

5 Results and discussion

5.1 Spatio-temporal variability of AOD in model simulation and observations

The model-simulated daily mean AODs were compared to AOD from ship-based remote sensing observations (Kedia and Ramachandran, 2008) and MODIS-derived Terra and Aqua satellite combined AOD values from 18 March to 10 May 2006 (Fig. 1). Model outputs were sampled along the cruise track to obtain daily-mean AOD at 550 nm matching the location and time periods of the cruise observations. AOD values derived from MODIS Terra and Aqua combined observations agree rather well in terms of variability ($R = 0.85$, see Table 1) with the sun photometer measured AOD values during ICARB period (Kedia and Ramachandran, 2008). ECHAM5.5-HAM simulated AOD variability agrees well with in-situ and satellite observations over the AS legs ($R = 0.88$ and $R = 0.77$, see Table 1) but the AOD was systematically underpredicted by up to a factor of 3 in high pollution episodes (18 March, 23 March, 24 March, 1 April, 2 April and 12 April) over the BoB legs (biases of −0.15 and −0.12 compared

Discussion Paper | Discussion Paper | Discussion Paper | Discussion Paper |

ACPD

11, 13911–13946, 2011

Examination of aerosol distributions and radiative effects

R. Cherian et al.

to the sunphotometer and MODIS, respectively; Table 1). Variability, however, still was relatively well simulated ($R = 0.68$ and $R = 0.75$, compared to the sunphotometer and MODIS, respectively; Table1 and Fig. 1). The difference in the AODs estimated by ship-based measurements and satellite measurements and model simulated AODs could arise due to the sampling time difference between the three systems (Sun photometer AOD was the mean AOD derived from 08:00 LST to 17:00 LST and MODIS AOD was the mean of 10:30 and 13:30 LST AODs, while model AOD was the 24-h average value). However, since MODIS retrievals of AOD at a $1^{\circ} \times 1^{\circ}$ resolution correspond well to the single-column ship-based sunphotometer measurements, and since also the sparse temporal sampling of MODIS (up to twice daily, depending on cloudiness) agrees well with the daytime-averages of the ship-based observations, we conclude that the AOD variability for this oceanic regions and season was low at temporal scales of less than 1 day, and at horizontal space scales of less than 1 degree.

The impact of aerosol swelling in high relative humidities during cloudy conditions, or of cloud contamination for both MODIS and sunphotometer observations, was examined with the help of the model by comparing the AOD values sampled at cloud-free days to the ones averaged over all days. Grid points with MODIS optical depth pixel counts greater than 20 are treated as cloud-free days. Seven days (25 March, 30 March, 2 April, 12 April, 21 April, 7 May and 10 May) were identified as cloud contaminated days since they show less than 20 valid MODIS AOD retrievals. The model simulated AOD agrees better with ship-based observations on cloud-free days compared to all days during the ICARB cruise period in terms of error (Root mean square error, RMSE of 0.13 vs. 0.16; Table S1) and in terms of variability ($R = 0.78$ vs. 0.69). The modelled total AOD was found to be underestimated by a factor of 1.92 (by 0.52) during cloudy days, compared to a small factor of 1.4 during cloud-free days. The Ångström exponent is relatively well simulated by the model (slightly overestimated compared to MODIS, on average by 5 %; see Table S5) on clear days. However, it was found to be over estimated by a factor of 1.28 (0.78 vs. 0.61) to 1.05 (0.99 vs. 0.94) during cloudy days compared to MODIS derived values. This indicates that particles

ACPD
11, 13911–13946, 2011

are too small in the model on cloudy days, leading to the conclusion that the simulated swelling of aerosol particles due to hygroscopic growth near cloudy areas is deficient, consistent with the low-bias were highly biased in model simulated AOD compared to MODIS observations during cloudy days (15 %). The fact that the ECHAM5.5-HAM model and MODIS AOD compare better in cloud-free situations corroborated this conclusion. Similar conclusions were found for the comparison between MODIS data and the sunphotometer, as well as when comparing the simulation to MODIS satellite retrievals. This indicates that swelling due to high relative humidity in cloudy situations and/or cloud contamination introduces additional variability, so that the single-column ship-based observations represent the large-scale MODIS retrievals only to a lesser extent.

The impact of the temporal vs. geographical evolution on the AOD values along the ship track was investigated to judge whether the AOD variability for the oceanic regions and season as observed during ICARB was representative of the entire region and season. This analysis was carried out using the two observational data sets (ship-based sunphotometer single-column measurements and MODIS satellite large-scale observations). Table S2 shows two ways of correlating ship-based sunphotometer data to large-scale MODIS retrievals: (i) sampling the MODIS data along the ship track – this was sampling the full spatio-temporal variability available from ICARB; and (ii) sampling MODIS data along the track, but from the seasonal mean AOD distribution – this was sampling only the geographical variability along the track. As expected, the spatial-only, seasonal-mean sampling from MODIS does not agree as well to the sunphotometer data in any of the statistical measures – particularly the large slope of the regression gets much worse. Still, we found that a large part of the variability was explained by the geographical variability, and the temporal variability (that is, specific pollution events) contribute only to a minor extent to the overall variability along the ICARB track (correlation coefficient $R = 0.50$ for the seasonal-mean sampling vs. 0.72 for the full spatio-temporal sampling along the track). Splitting this up, we found that in the BoB, individual events were more important than in the AS region, where even the

ACPD
11, 13911–13946, 2011

correlation coefficient was slightly larger for seasonal-mean sampling (a result probably just showing a statistical uncertainty in the correlation coefficient).

For evaluating the spatial distribution of model simulated aerosol optical properties, the mean (averaged from 18 March to 10 May) of the model derived AOD at 550 nm was compared to mean MODIS satellite observations (Fig. 2). Both simulated and satellite-retrieved AODs were found to be high close to the coast and near populated urban locations. Over the BoB, a clear gradient was seen, with AOD decreasing from northeast to southwest (Fig. 2) and the high AOD values were mainly attributed to continental outflow from the Indo-Gangetic Plain (IGP) and east Asia, as well as long-range transport of mineral dust aerosols from the west Asian regions. This gradient was captured well by the model, which, however, shows an overall underestimation quantitatively. The high values of simulated AODs along the Mangalore coast appear to be a consistent feature over the AS region along with ICARB observations (Moorthy et al., 2008), and were reported during several earlier cruise studies (Parameswaran et al., 1999; Moorthy and Saha, 2000; Ramachandran, 2004), which was also captured in satellite observations (Fig. 2). However, the simulated plume does not extend far enough to the North, but, on the other hand, extends too far off shore. The analysis of simulated spatial distributions of individual aerosol species showed that a sulfate plume extending from south east India to the AS and dust plumes extending from west Asia and western India to the AS resulted in high AODs near the Mangalore coast during ICARB period. Receptor modelling analysis also showed that this period was associated with an increased outflow from west Asia and western coast of India (Cherian et al., 2010), more subject to dust emissions. The spatial distribution of simulated AOD agrees well ($R = 0.8$, see Table 1) with MODIS observations in most of the AS regions. Over the BoB region, it was systematically underestimated by a factor of 1.5, specifically near coastal regions (Fig. 2), but variability still was relatively well captured ($R = 0.75$). For understanding the model discrepancies in aerosol representation, the simulated AOD was examined for the different modes which were discussed in the following sections.

ACPD
11, 13911–13946, 2011

5.2 Fine and coarse mode AOD

To understand the model underprediction in more detail, the modelled AODs at 550 nm were compared with satellite observations (MODIS, Terra & Aqua combined) in fine and coarse modes (see Fig. 3). MODIS fine and coarse mode AOD was derived using the MODIS AOD and fine mode fraction (FMF) values. HAM fine mode AOD was estimated by adding the Aitken and accumulation mode (both soluble and insoluble modes) AODs. Both simulated fine and coarse mode AODs agree rather well ($R = 0.8$ and $R = 0.6$, Table1) with MODIS fine and coarse mode AODs over the AS legs in terms of variability, but showed a certain underestimation quantitatively, especially for a few days, where in particular the coarse mode was substantially underestimated (Fig. 3). During the BoB leg, most of the fine mode AODs were underpredicted by up to a factor of 2 to 3, while coarse mode AODs were occasionally significantly underpredicted by a factor of 3 to 6 (Fig. 3) with a regression slope as low as 0.09 (Table 1). The reasons for the underestimation of both fine and coarse AODs are discussed later. The variability in the fine mode was acceptably well simulated also for the BoB leg ($R = 0.65$), but severely wrong for the coarse mode ($R = 0.24$).

The significant underestimation of fine and, particularly, coarse mode AODs during BoB leg may result from incorrect aerosol emissions, or aerosol transport. To examine this further, the chemical composition for fine and coarse mode column burden was analysed (see Fig. S1). It was found that the anthropogenic aerosols (sulfate and, to a lesser extent, organic carbon), dominate (50–80 %) the fine mode column burden, with the remaining parts mostly due to aerosol water uptake, and negligible contributions from dust, black carbon and sea salt. Natural aerosols (dust and, to a much lesser extent, sea salt) were dominant (90 %) to the coarse mode column burden during these periods (see Fig. S1). Especially over the AS leg, water was found to be a large contributor to the coarse-mode column burden as well. Back trajectory and receptor model analysis showed that air mass during this period was associated with an outflow from the Indo-Gangetic plain or central India (anthropogenic aerosols) and the western

ACPD
11, 13911–13946, 2011

India or Arabia (dust emissions) (Cherian et al., 2010). However, the impact of the continental advection decreased continuously as the ship moved southwards. In the model, the emission of mineral dust depends on the online prognostic wind speed at 10 m above the surface and the prescribed surface feature of soils (Stier et al., 2005). Some of the observed coarse mode AOD may stem from dust emissions, which were not well represented, or not included at all, in the model. This may also contribute to the underestimation of coarse mode AODs during the BoB legs. Deficiencies in the simulation of aerosol transport and processing may also contribute. The limited number of in-situ observations might reduce the quality of ECMWF reanalysis data over the Indian Ocean region (Bonazzola et al., 2001), potentially biasing the wind fields used for nudging in the ECHAM5.5-HAM simulations. This reduces the fidelity of the transport of continental anthropogenic aerosols to the BoB regions, thus contributing to the underestimation of the fine AODs over these regions.

To examine dust AOD underestimation further, the simulated dust AOD was compared with the satellite derived UV AI during the BoB leg (Fig. 4). It was found that the missing of Thar desert dust plumes during 18 March, 19 March, 1 April and 2 April periods resulted in very low dust coarse mode AODs (∼0.03), with an underprediction by a factor of 5 during these days (Fig. 3). The missing dust source, affected the AOD values along cruise prediction on 4 out of 23 days during the BoB cruise (a fraction of 17 %). During these four days the modelled total AOD was found to be underestimated by a factor of 2.27, compared to a smaller bias (under estimation by a factor of 1.42) when analyzing the entire period (Table S6). At the same time, UV AI values over the Thar desert region confirm the existence of significant dust outbreak events (Fig. 4). The AI indeed exceeds a value of 1.0 in the region of the Thar desert, signifying the existence of aerosols absorbing UV radiation. Such approaches were previously used to identify missing dust source episodes (Flaounas et al., 2009). The fact that the model compares better in average situations compared to missing-dust source days points to the inaccuracies in simulating enough dust emission flux during these days. Even if in general, the model simulated dust AOD in the same locations where the UV Aerosol

Index (AI) indicates dust source regions (Arabian peninsula, Thar desert), relatively little dust was transported to the ship location from the northern Indian subcontinent. This anomalous transport results in rather low coarse mode AOD in most of the BoB cruise days (Fig. 4). Finally, there might be a mis-representation of aerosol wet scavenging and sedimentation. To examine this further, the wet and dry deposition flux of dust aerosols were analysed during the entire BoB cruise period and separately for the average of 4 days where the model failed to capture large values of coarse-mode AODs. It was found that the fraction of dust removed from the atmosphere by both dry and wet deposition is comparable during the days where the model lacks dust and the average over the BoB period (Fig. S4). Also the aging of dust due to microphysical processing is not very different in the four days with the low-bias in dust. However, a particularly low model dust emission flux was found during these 4 days over the Thar desert (north west India) region (Fig. S3). This points to possible inaccuracies in surface wind fields in this region. The lack of precise maps of surface features in Asian regions, especially the soil clay content and erodible fraction of the surface, and not well resolved secondary dust sources and regional topography may also result in the underestimation of coarse mode dust AODs (Cheng et al., 2008). Therefore underestimation of AOD (mainly coarse AOD) in high AOD periods mainly stem from missing aerosol sources (most probably was coarse mode dust – mainly in Thar Desert areas – but also fine mode sulfate and OC) and incorrect aerosol transport. Though ECHAM5.5-HAM AOD estimates were underestimated in high pollution episodes (especially over the BoB regions), the model still is a valuable tool to understand the mean pre-monsoon aerosol size distribution, atmospheric absorption, and radiative effects during the ICARB period.

5.3 Ångström exponent

The spatial distribution of the simulated Ångström exponent (α, 550 nm/825 nm) was evaluated using the satellite retrieved Ångström exponent from the MODIS sensor (550 nm/865 nm, Terra and Aqua combined) during the ICARB cruise period (Fig. S2).

ACPD
11, 13911–13946, 2011

Some features of the geographical distribution of the simulated α agrees well with satellite observations over the AS regions. Low Ångström exponent values (large particle sizes) were simulated in the northern AS region, in close agreement with the satellite retrievals. Also the pattern of the north-east to south-west decreasing gradient α (increasing particle sizes) moving away from the coast was well represented. However, the model consistently overestimates α, or underestimates aerosol particle size, consistent with the above finding of too little simulated dust concentrations. Over the BoB, the model showed far too little variability, and – as for the AS region – particle sizes were underestimated. The overall gradient of increasing particle sizes moving away from the Indian coast, though, was simulated. High values of α (1–1.5) were found over the BoB leg indicating a relatively large fraction of fine mode particles (Fig. S2), while large heterogeneities found over AS leg with relatively small values (<1) of α (Fig. S2). The southern AS (south of 14° N) was characterized by high values of α with values in the range 0.6 to 0.8 (0.85 to 1 in the model), indicating high relative abundance of accumulation mode (sulfate) aerosols (Fig. S2). Compared to this, the northern AS (north of 15° N) was dominated by coarser mode aerosols (dust) and α value in the range 0.45 to 0.75, consistent in both model and satellite retrievals (Fig. S2). The coarse mode aerosols were mainly associated with mineral dust (see previous section and Fig. S1). The percentage contribution of fine mode (accumulation + Aitken) particles to total AODs was found to be high (68 %) – this also shows the dominance of fine mode aerosols (sulfate and OC aerosols in accumulation soluble mode) over the BoB legs in the model, indicating the transport from IGP and central India regions (see Table S3). This was consistent with findings based on measurements (Kedia and Ramachandran, 2008), which showed larger AODs and FMFs, and receptor modeling (Cherian et al., 2010), which showed the predominance of anthropogenic factors, during the cruise over the BoB when the ship was mainly influenced by air masses from the IGP or central India.

ACPD
11, 13911–13946, 2011

5.4 Aerosol absorption and radiative forcing

Aerosol absorption determines the amount of solar heating by atmospheric aerosol and may be quantified by the aerosol absorption optical depth (AAOD), which is defined as the product of the AOD and aerosol single scattering co-albedo. For evaluating the spatial distribution of aerosol absorption, the mean (averaged over the 18 March to 10 May period) simulated AAOD at 550 nm was compared to OMI (aboard EOS-Aura) retrieved AAOD at 500 nm (Fig. 5). High AAOD values were found over the biomass regions of India and east Asia regions (Fig. 5). Good agreement for the geographical distribution of absorption was found for large AOD regions over land between OMI and simulated AAOD values, while OMI AAOD was found to be very low over most of the oceanic regions (Fig. 5). However, OMI retrievals carry a significant uncertainty with likely underestimation of AAOD at low AOD values as those observed over the ocean. The uncertainty in satellite retrieval was mainly associated with the assumed aerosol layer height (Torres et al., 2007), aerosol type misidentification (3 basic types such as dust, carbonaceous aerosols and weakly absorbing sulfates, Torres et al., 2007) and cloud contamination (Torres et al., 2007). The model showed that absorption of solar radiation by aerosols was mostly due to BC (about 80 % to 90 %) over the oceans and continent regions, with remaining portion accounted for by mineral dust and OC (see Fig. 5c–d).

The model simulated short-wave (SW) clear-sky direct aerosol radiative forcing (DARF) at the TOA (ΔF_{TOA}), surface (ΔF_{SUR}) and, within the atmosphere ($\Delta F_{ATM} = \Delta F_{TOA} - \Delta F_{SUR}$) was analysed to determine the aerosol direct radiative effects during ICARB period. The simulated mean DARF sampled along the ship track over BoB leg was found to be −4.7, −11.3, and 6.6 W m^{-2} at TOA, SUR, and ATM, while that over AS was −6.1, −10.7, and 4.6 W m^{-2} at TOA, SUR, and ATM (Table S4). The model simulated regional-seasonal mean DARF was compared to the DARF sampled along the ship track to analyse to which extent the ICARB cruise was representative of the entire region/pre-monsoon season. The regional-seasonal mean simulated DARF over the

ACPD
11, 13911–13946, 2011

BoB was $-4.2\,\mathrm{W\,m^{-2}}$, $-9.8\,\mathrm{W\,m^{-2}}$, and $+5.6\,\mathrm{W\,m^{-2}}$ at TOA, SUR, and ATM, respectively; and −6.0, -10.7, and $+4.7\,\mathrm{W\,m^{-2}}$ over the AS leg. On average, thus, the forcings sampled along the ship track were consistent with the ones obtained for the entire region and pre-monsoon season to within $\pm0.5\,\mathrm{W\,m^{-2}}$, $\pm1.5\,\mathrm{W\,m^{-2}}$ and $\pm1\,\mathrm{W\,m^{-2}}$ at TOA, SUR, and ATM, respectively, with much less discrepancy over the AS than over the BoB. Since the regional-seasonal mean DARF sampled along the ICARB ship track corresponds so well to the temporal and seasonal mean DARF over both the BoB and, even more so, AS regions, we conclude that the ICARB cruise track was well chosen to be representative of the entire region and the season.

Above, we showed that the model was underestimating AOD values, especially for dust and in high pollution episodes. Thus, the simulated DARF was likely to be underestimated as well. We thus use the observations to obtain constrained, improved DARF estimates. A satellite-tied DARF was calculated by multiplying model simulated seasonal mean forcing efficiency (DARF per unit AOD) with MODIS AOD. A sunphotometer-tied DARF was calculated also, by multiplying the simulated seasonal mean forcing efficiency with the ICARB ship-based AOD along the ship track (Table 2). As expected, the forcing increases in absolute terms, particularly over the BoB, where observed AODs were larger than the simulated ones. Sunphotometer-tied forcings along the cruise track were somewhat larger than satellite-tied ones, consistent with what we found earlier from the model (Table S2). This forcing estimate, revised using the observations, yields a regional-seasonal mean anthropogenic forcing of −5.6 and $-2.3\,\mathrm{W\,m^{-2}}$ at the TOA and at the surface. The unconstrained model underestimated the TOA and surface forcing by a factor of 1.4. This indicates the magnitude of model uncertainty in the estimation of aerosol radiative forcing. As a best estimate, the regional-mean seasonal-mean forcing, as obtained by the satellite-tied computation, in the BoB region −8.6, −21.4, and $+12.9\,\mathrm{W\,m^{-2}}$ at TOA, SUR, and ATM, respectively, and in the AS region is , −6.8, −12.8, and $+6.0\,\mathrm{W\,m^{-2}}$ at TOA, SUR, and ATM, respectively. The forcing along the track can be compared to the published values for the ICARB campaign from Kedia et al. (2010), which we list in Table 2. The sunphotometer-

ACPD
11, 13911–13946, 2011

tied values were much closer – within about ±2 $W m^{-2}$, except for the ATM forcing over the BoB, where the discrepancy was 4 $W m^{-2}$ – to the one Kedia et al. (2010) obtained than the model-only estimates.

The spatial variations of the seasonal-mean DARF, as obtained by the satellite-tied computation, at TOA, SUR and ATM during the ICARB period are shown in Fig. 6. Large spatial heterogeneity in DARF was observed in both BoB and AS regions consistent with AOD patterns over both regions. Over the BoB region, the atmospheric forcing was found to be high when the ship was moving near the northern BoB, while over AS the forcing was high when the ship was moving near the southern Indian peninsula. This was consistent with the ICARB cruise observations (Kedia et al., 2010; Moorthy et al., 2009). The TOA forcing was negative over most of oceanic regions except over regions with bright surfaces (desert and ice regions). Significant cooling was simulated at the TOA (−2 to −10 $W m^{-2}$) and at the SUR (−5 to −25 $W m^{-2}$) over the BoB and AS regions, which compares well with previous GCM estimates (Reddy et al., 2004). The ATM forcing decreased continuously with latitude from ≥15 $W m^{-2}$ to 5 $W m^{-2}$ as was reported in ICARB cruise studies (Moorthy et al., 2009).

The normalized direct radiative forcing or direct radiative forcing efficiency (ARFE, $W m^{-2} \tau^{-1}$) determines the efficiency of the aerosols to interact with the radiation and indicates the aerosol type and its absorption efficiency (Moorthy et al., 2009). It is defined as the ATM forcing ($W m^{-2}$) per unit AOD at 550 nm. The aerosols capable of imparting higher ATM forcing were located in the IGP, central India, eastern India and east Asia regions (Fig. 6d). Interestingly over coastal regions which are rich in aerosols, only northern BoB, northwestern AS and southern BoB regions were found to have high atmospheric absorption efficiency indicating that the presence of more absorbing type (BC and dust) aerosols. While high AOD regions such as off the coast of Mangalore show low forcing efficiency indicating the presence of more scattering type aerosols (mainly sulfates).

The ratio (f_s) of the surface forcing to the TOA forcing gives an indication to the aerosol type (scattering or absorbing). Generally the values of f_s>∼3 represent strong influence of absorbing aerosols while for scattering aerosols f_s<2 (Podgorny et al., 2000). The ratio ranges from 2 to 3 over the BoB and 1 to 2 over the AS, which compares well (2 to 3) with the previous estimates (Moorthy et al., 2009) and reveals the dominance of the surface forcing and scattering aerosols (sulfates, organic carbon, and sea salt) over most of the oceanic regions. High f_s values (>5) found over the polluted regions (northeastern India and east Asia regions) indicate the dominance of absorbing aerosols, which mainly resulted from biomass burning and forest burning.

Studies from the ICARB campaign have showed large abundances of aerosols over the BoB and AS regions. However, studies addressing the distribution of atmospheric heating rates are still sparse. The spatial distribution of solar heating rate (K/day) was examined to provide a better understanding of the aerosol influence on atmospheric heating patterns, sampled here for the ICARB period (Fig. 7). There is a high south-north gradient in BC absorption optical depth during this period over the BoB (Fig. 5) pointing to greater columnar abundance of absorbing aerosols in the northern BoB. In addition, there is presence of an elevated aerosol layer, both of BC and dust in the northern BoB (Fig. S5). It was found that the simulated BC aerosol concentration showed an elevated layer peaking at around 3 km in the northern BoB region (Reaction R1), while only a small peak at 1 km was found in the southern BoB region (Reaction R2) (Fig. S5). It is known that elevated absorbing aerosols, especially where located above low-level clouds, lead to particularly large heating rates due to the additional absorption of back scattered radiation. An uncertainty associated with previous heating rate estimates was due to the assumption that the dominant part of the atmospheric aerosol concentrations was found in surface up to 4 km. This assumption is justified by the model simulated regional-mean concentrations where 85–90 % of the total aerosol concentrations were found below 4 km. The mean solar heating rate was found to be larger over the BoB region (0.29 K/d, see Table 2) than over the AS region (0.17 K/d), which was comparable with the value obtained in ICARB cruise studies (Kedia et al., 2010; Moorthy et al., 2009).

ACPD
11, 13911–13946, 2011

Discussion Paper | Discussion Paper | Discussion Paper | Discussion Paper |
Title Page
Abstract Introduction
Conclusions References
Tables Figures
◀◀ ▶▶
◀ ▶
Back Close
Full Screen / Esc
Printer-friendly Version
Interactive Discussion

6 Conclusions

This study analyses ship-based sun-photometer measurements of aerosol optical depth from the ICARB field campaign over the BoB and the AS region together with a nudged simulation of the large-scale aerosol-climate model ECHAM5.5-HAM and several satellite data sets. The model has been evaluated by a comparison with in situ measurements from ships, and with satellites (MODIS and OMI). The model reproduces the large spatial and temporal heterogeneities in the aerosol optical depth during ICARB period. Simulated variability agrees rather well with both in-situ and satellite observations ($R = 0.8$) during AS legs. However, the model cannot reproduce (underprediction by a factor of 3) the large AODs observed during high pollution days, especially over the BoB legs. Since MODIS retrievals of AOD correspond well to the ship-based sunphotometer measurements, and since also the sparse sampling of MODIS (up to twice daily, depending on cloudiness) agrees well with the diurnal averages of the ship-based observations, we conclude that the AOD variability for this oceanic region and season was low at temporal scales of less than 1 day, and at horizontal space scales of less than 1 degree. The HAM simulated AOD agrees better with the ship-based sunphotometer measurements and satellite measurements during cloud-free days when compared to all days indicating enhanced spatio-temporal AOD variability due to aerosol swelling resulted from larger humidity and/or retrieval errors in cloudy situations.

HAM simulated fine and coarse mode AODs at 550 nm were evaluated with MODIS retrievals to better understand the model performance over the BoB and AS legs. The HAM fine mode AODs were underpredicted by a factor of 2 as compared to satellite observations, while coarse mode AODs were strongly underestimated by a factor of 3 to 6 over the BoB region. The analysis of dust AOD along with the UV AI from OMI sensor showed deficiencies of dust source regions (Thar Desert) and the model dust transport from northern India, potentially due to uncertainties in ECMWF wind fields. This caused an underestimation of coarse mode AODs over BoB regions. The fine

Discussion Paper | Discussion Paper | Discussion Paper | Discussion Paper |

ACPD
11, 13911–13946, 2011

Examination of aerosol distributions and radiative effects

R. Cherian et al.

and coarse mode AODs were predicted better over the AS region except for a few days where the model wind fields transported fine and coarse mode aerosols from west Asia and central and southern India to the surrounding oceanic regions. In these cases, a significant underestimation of super-micron dust AODs resulted in the underestimation of AODs in high pollution days over the BoB legs.

Aerosol radiative forcing and atmospheric heating rates exhibit large spatial heterogeneities over the BoB and AS regions. The regional-seasonal mean shortwave DARF was found to correspond well to DARF sampled along the BoB and AS region ship cruise. In conclusion, the ICARB cruise was well chosen to be representative of direct aerosol radiative effects for the entire region and the season. Taking into account the model deficiencies (underprediction of AOD) by constraining radiative effect computations with observations, the mean DARF over the BoB was estimated as −8.6, −21.4 and +12.9 $\mathrm{W\,m^{-2}}$ at TOA, SUR, and ATM, and over the AS, −6.8, −12.8, and +6 at TOA, SUR, and ATM, respectively. The spatial heterogeneity of aerosol radiative forcing resembles that of the AOD; while the spatial variability of atmospheric forcing efficiency was similar to that of the AAOD. The average solar heating rate was found to be larger over the BoB region (0.3 K/d) when compared to AS region (0.17 K/d).

Supplement related to this article is available online at:
http://www.atmos-chem-phys-discuss.net/11/13911/2011/acpd-11-13911-2011-supplement.pdf.

Acknowledgements. This work was supported through the Atmospheric Trace Gases-Chemistry, Transport and Modeling (AT-CTM) project of the Indian Space Research Organisation's Geosphere Biosphere Programme (ISRO-GBP), Bengaluru, India. The satellite data used in this study are downloaded from GES-DISC, NASA. Computing time was provided by the German High Performance Computing Centre for Climate and Earth System Research (Deutsches Klimarechenzentrum, DKRZ). We thank Kai Zhang (Max Planck Institute for Meteorology) for carefully reviewing the manuscript. J. Quaas was supported by an Emmy Noether grant of the German Research Foundation (DFG). R. Cherian acknowledges the funding support from the Guest-Exchange program of the International Max Planck Research School on Earth System Modelling (IMPRS-ESM) for his visit to MPI-M (Hamburg, Germany).

The service charges for this open access publication
have been covered by the Max Planck Society.

References

Adhikary, B., Carmichael, G. R., Tang, Y., Leung, L. R., Qian, Y., Schauer, J. J., Stone, E. A., Ramanathan, V., and Ramana, M. V.: Characterization of the seasonal cycle of south Asian aerosols: A regional-scale modeling analysis, J. Geophys. Res., 112, D22S22, doi:10.1029/2006JD008143, 2007.

Andres, R. J. and Kasgnoc, A. D.: A time-averaged inventory of subaerial volcanic sulfur emissions, J. Geophys. Res., 103, 25251–25261, 1998.

Bonazzola, M., Picon, L., Laurent, H., Hourdin, F., Séze, G., Pawlowska, H., and Sadourny, R.: Retrieval of large-scale wind divergences from infrared Meteosat-5 brightness temperatures over the Indian Ocean, J. Geophys. Res., 106, 28113–28128, 2001.

Cheng, T., Peng, Y., Feichter, J., and Tegen, I.: An improvement on the dust emission scheme in the global aerosol-climate model ECHAM5-HAM, Atmos. Chem. Phys., 8, 1105–1117, doi:10.5194/acp-8-1105-2008, 2008.

Cherian, R., Venkataraman, C., Kumar, A., Sarin, M. M., Sudheer, A. K., and Ramachandran, S.: Source identification of aerosols influencing atmospheric extinction: Integrating PMF and PSCF with emission inventories and satellite observations, J. Geophys. Res., 115, D22212, doi:10.1029/2009JD012975, 2010.

Chung, C. E., Ramanathan, V., Kim, D., and Podgorny, I. A.: Global anthropogenic aerosol direct forcing derived from satellite and ground-based observations, J. Geophys. Res., 110, D24207, doi:10.1029/2005JD006356, 2005.

Cofala, J., Amann, M., and Mechler, R.: Scenarios of world anthropogenic emissions of air pollutants and methane up to 2030, International Institute for Applied Systems Analysis (IIASA)), Laxenburg, Austria, 2005.

Dentener, F., Kinne, S., Bond, T., Boucher, O., Cofala, J., Generoso, S., Ginoux, P., Gong, S., Hoelzemann, J. J., Ito, A., Marelli, L., Penner, J. E., Putaud, J. P., Textor, C., Schulz, M., van der Werf, G. R., and Wilson, J.: Emissions of primary aerosol and precursor gases in the years 2000 and 1750 prescribed data-sets for AeroCom, Atmos. Chem. Phys., 6, 4321–4344, doi:10.5194/acp-6-4321-2006, 2006.

Feichter, J., Kjellstrom, E., Rodhe, H., Dentener, F., Lelieveld, J., and Roelofs, G. J.: Simulation of the tropospheric sulfur cycle in a global climate model, Atmos. Environ., 30, 1693–1707, 1996.

Flaounas, E., Coll, I., Armengaud, A., and Schmechtig, C.: The representation of dust transport and missing urban sources as major issues for the simulation of PM episodes in a Mediterranean area, Atmos. Chem. Phys., 9, 8091–8101, doi:10.5194/acp-9-8091-2009, 2009.

Forster, P., Ramaswamy, V., Artaxo, P., Berntsen, T., Betts, R., Fahey, D. W., Haywood, J., Lean, J., Lowe, D. C., Myhre, G., Nganga, J., Prinn, R., Raga, G., Schulz, M., and Dorland, R. V.: Changes in atmospheric constituents and in radiative forcing in: Climate Change 2007: The Physical Science Basis-Contribution of Working Group I to the Fourth Assessment Report of the Intergovernmental Panel on Climate Change, edited by: Solomon, S., Qin, D., Manning, M., Chen, Z., Marquis, M., Averyt, K. B., Tignor, M., and Miller, H. L., Cambridge Univ. Press, Cambridge, UK, 153–171, 2007.

Kahn, R. A., Garay, M. J., Nelson, D. L., Yau, K. K., Bull, M. A., Gaitley, B. J., Martonchik, J. V., and Levy, R. C.: Satellite-derived aerosol optical depth over dark water from MISR and MODIS: Comparisons with AERONET and implications for climatological studies, J. Geophys. Res., 112, D18205, doi:10.1029/2006JD008175, 2007.

Kedia, S. and Ramachandran, S.: Features of aerosol optical depths over the Bay of Bengal and the Arabian Sea during premonsoon season: Variabilities and anthropogenic influence, J. Geophys. Res., 113, D11201, doi:10.1029/2007JD009070, 2008.

Kedia, S., Ramachandran, S., Kumar, A., and Sarin, M. M.: Spatiotemporal gradients in aerosol radiative forcing and heating rate over Bay of Bengal and Arabian Sea derived on the basis of optical, physical, and chemical properties, J. Geophys. Res., 115, D07205, doi:10.1029/2009JD013136, 2010.

Kinne, S., Schulz, M., Textor, C., Guibert, S., Balkanski, Y., Bauer, S. E., Berntsen, T., Berglen, T. F., Boucher, O., Chin, M., Collins, W., Dentener, F., Diehl, T., Easter, R., Feichter, J., Fillmore, D., Ghan, S., Ginoux, P., Gong, S., Grini, A., Hendricks, J. E., Herzog, M., Horowitz, L., Isaksen, L., Iversen, T., Kirkavag, A., Kloster, S., Koch, D., Kristjansson, J. E., Krol, M., Lauer, A., Lamarque, J. F., Lesins, G., Liu, X., Lohmann, U., Montanaro, V., Myhre, G., Penner, J. E., Pitari, G., Reddy, S., Seland, O., Stier, P., Takemura, T., and Tie, X.: An

ACPD
11, 13911–13946, 2011

Examination of aerosol distributions and radiative effects

R. Cherian et al.

AeroCom initial assessment – optical properties in aerosol component modules of global models, Atmos. Chem. Phys., 6, 1815–1834, doi:10.5194/acp-6-1815-2006, 2006.

Koch, D., Bond, T. C., Streets, D., Unger, N., and van der Werf, G. R.: Global impacts of aerosols from particular source regions and sectors, J. Geophys. Res., 112, D02205, doi:10.1029/2005JD007024, 2007.

Liou, K. N.: An Introduction to Atmospheric Radiation, San Diego, CA, USA, 392 pp., 1980.

Moorthy, K. K. and Saha, A.: Aerosol study during INDOEX: observation of enhanced aerosol activity over the Mid Arabian Sea during the northern winter, J. Atmos. Solar-Terr. Phys., 62, 65–72, 2000.

Moorthy, K. K., Satheesh, S. K., Babu, S. S., and Dutt, C. B. S.: Integrated campaign for aerosols, gases and radiation budget (ICARB): An overview, J. Earth Syst. Sci., 117, 243–262, 2008.

Moorthy, K. K., Nair, V. S., Babu, S. S., and Satheesh, S. K.: Spatial and vertical heterogeneities in aerosol properties over oceanic regions around India: Implications for radiative forcing, Q. J. Roy. Meteorol. Soc., 135, 2131–2145, 2009.

Parameswaran, K., Nair, P. R., Rajan, R., and Ramana, M. V.: Aerosol loading in coastal and marine environments in the Indian Ocean region during winter season, Curr. Sci., 76, 947–955, 1999.

Podgorny, I. A., Conant, W., Ramanathan, V., and Satheesh, S. K.: Aerosol modulation of atmospheric and surface solar heating over the tropical Indian Ocean, Tellus Series B-Chem. Phys. Meteorol., 52, 947–958, 2000.

Ramachandran, S.: Spectral aerosol optical characteristics during the northeast monsoon over the Arabian Sea and the tropical Indian Ocean: 1. Aerosol optical depths and their variabilities, J. Geophys. Res., 109, D19207, doi:10.1029/2003JD004476, 2004.

Ramachandran, S. and Jayaraman, A.: Premonsoon aerosol mass loadings and size distributions over the Arabian Sea and the tropical Indian Ocean, J. Geophys. Res., 107, 4738, doi:10.1029/2002JD002386, 2002.

Ramachandran, S. and Cherian, R.: Regional and seasonal variations in aerosol optical characteristics and their frequency distributions over India during 2001-2005, J. Geophys. Res., 113, D08207, doi:10.1029/2007JD008560, 2008.

Ramanathan, V., Crutzen, P. J., Lelieveld, J., Mitra, A. P., Althausen, D., Anderson, J., Andreae, M. O., Cantrell, W., Cass, G. R., Chung, C. E., Clarke, A. D., Coakley, J. A., Collins, W. D., Conant, W. C., Dulac, F., Heintzenberg, J., Heymsfield, A. J., Holben, B., Howell, S., Hudson,

ACPD

11, 13911–13946, 2011

Examination of aerosol distributions and radiative effects

R. Cherian et al.

J., Jayaraman, A., Kiehl, J. T., Krishnamurti, T. N., Lubin, D., McFarquhar, G., Novakov, T., Ogren, J. A., Podgorny, I. A., Prather, K., Priestley, K., Prospero, J. M., Quinn, P. K., Rajeev, K., Rasch, P., Rupert, S., Sadourny, R., Satheesh, S. K., Shaw, G. E., Sheridan, P., and Valero, F. P. J.: Indian Ocean Experiment: An integrated analysis of the climate forcing and effects of the great Indo-Asian haze, J. Geophys. Res., 106, 28371–28398, 2001.

Reddy, M. S. and Venkataraman, C.: Inventory of aerosol and sulphur dioxide emissions from India: I - Fossil fuel combustion, Atmos. Environ., 36, 677–697, 2002.

Reddy, M. S., Boucher, O., Venkataraman, C., Verma, S., Leon, J. F., Bellouin, N., and Pham, M.: General circulation model estimates of aerosol transport and radiative forcing during the Indian Ocean Experiment, J. Geophys. Res., 109, D16205, doi:10.1029/2004JD004557, 2004.

Reddy, M. S., Boucher, O., Balkanski, Y., and Schulz, M.: Aerosol optical depths and direct radiative perturbations by species and source type, Geophys. Res. Lett., 32, L12803, doi:10.1029/2004GL021743, 2005.

Remer, L. A., Kaufman, Y. J., Tanre, D., Mattoo, S., Chu, D. A., Martins, J. V., Li, R. R., Ichoku, C., Levy, R. C., Kleidman, R. G., Eck, T. F., Vermote, E., and Holben, B. N.: The MODIS aerosol algorithm, products, and validation, J. Atmos. Sci., 62, 947–973, 2005.

Roeckner, E.: The atmospheric general circulation model ECHAM5. PART I: Model description, Max Planck Institute for Meteorology, Hamburg, Germany, Report 349, 1–140, 2003.

Schulz, M., G., Leeuw, D., and Balkanski, Y.: Emission of Atmospheric Trace Compounds, Chap. Sea-salt aerosol source functions and emissions, edited by: Kluwer, 333–359, 2004.

Simmons, A. J. and Gibson, J. K.: The ERA-40 project plan, ERA-40 Project Report Series 1, ECMWF, Shinfield Park, Reading, UK., 2000.

Stier, P., Feichter, J., Kinne, S., Kloster, S., Vignati, E., Wilson, J., Ganzeveld, L., Tegen, I., Werner, M., Balkanski, Y., Schulz, M., Boucher, O., Minikin, A., and Petzold, A.: The aerosol-climate model ECHAM5-HAM, Atmos. Chem. Phys., 5, 1125–1156, doi:10.5194/acp-5-1125-2005, 2005.

Stier, P., Feichter, J., Kloster, S., Vignati, E., and Wilson, J.: Emission-induced nonlinearities in the global aerosol system: Results from the ECHAM5-HAM aerosol-climate model, J. Climate., 19, 3845–3862, 2006.

Stier, P., Seinfeld, J. H., Kinne, S., and Boucher, O.: Aerosol absorption and radiative forcing, Atmos. Chem. Phys., 7, 5237–5261, doi:10.5194/acp-7-5237-2007, 2007.

Tegen, I., Harrison, S. P., Kohfeld, K., Prentice, I. C., Coe, M., and Heimann, M.: Impact of

ACPD
11, 13911–13946, 2011

Examination of aerosol distributions and radiative effects

R. Cherian et al.

vegetation and preferential source areas on global dust aerosol: Results from a model study, J. Geophys. Res., 107, 4576, doi:10.1029/2001JD000963, 2002.
Textor, C., Schulz, M., Guibert, S., Kinne, S., Balkanski, Y., Bauer, S., Berntsen, T., Berglen, T., Boucher, O., Chin, M., Dentener, F., Diehl, T., Easter, R., Feichter, H., Fillmore, D., Ghan, S., Ginoux, P., Gong, S., Kristjansson, J. E., Krol, M., Lauer, A., Lamarque, J. F., Liu, X., Montanaro, V., Myhre, G., Penner, J., Pitari, G., Reddy, S., Seland, O., Stier, P., Takemura, T., and Tie, X.: Analysis and quantification of the diversities of aerosol life cycles within AeroCom, Atmos. Chem. Phys., 6, 1777–1813, doi:10.5194/acp-6-1777-2006, 2006.
Toon, O. B. and Ackerman, T. P.: Algorithms for the Calculation of Scattering by Stratified Spheres, Appl. Opt., 20, 3657–3660, 1981.
Torres, O., Tanskanen, A., Veihelmann, B., Ahn, C., Braak, R., Bhartia, P. K., Veefkind, P., and Levelt, P.: Aerosols and surface UV products from Ozone Monitoring Instrument observations: An overview, J. Geophys. Res., 112, D24S47, doi:10.1029/2007JD008809, 2007.
Venkataraman, C., Habib, G., Eiguren-Fernandez, A., Miguel, A. H., and Friedlander, S. K.: Residential biofuels in south Asia: Carbonaceous aerosol emissions and climate impacts, Science, 307, 1454–1456, 2005.
Venkataraman, C., Habib, G., Kadamba, D., Shrivastava, M., Leon, J. F., Crouzille, B., Boucher, O., and Streets, D. G.: Emissions from open biomass burning in India: Integrating the inventory approach with high-resolution Moderate Resolution Imaging Spectroradiometer (MODIS) active-fire and land cover data, Global Biogeochem. Cy., 20, GB2013, doi:10.1029/2005GB002547, 2006.
Verma, S., Venkataraman, C., and Boucher, O.: Origin of surface and columnar Indian Ocean Experiment (INDOEX) aerosols using source- and region-tagged emissions transport in a general circulation model, J. Geophys. Res., 113, D24211, doi:10.1029/2007JD009538, 2008.
Vignati, E., Wilson, J., and Stier, P.: M7: An efficient size-resolved aerosol microphysics module for large-scale aerosol transport models, J. Geophys. Res., 109, D22202, doi:10.1029/2003JD10041485, 2004.

ACPD
11, 13911–13946, 2011

ACPD
11, 13911–13946, 2011

Examination of aerosol distributions and radiative effects

R. Cherian et al.

Title Page
Abstract | Introduction
Conclusions | References
Tables | Figures
◀I | ▶I
◀ | ▶
Back | Close
Full Screen / Esc
Printer-friendly Version
Interactive Discussion

Table 1. Linear regression statistics between the ship-based remote sensing measurements, MODIS observations and model simulated AODs over the Bay of Bengal and Arabian Sea legs during ICARB cruise period.

Region	Statistics	Sunphotometer vs. MODIS	Sunphotometer vs. HAM	MODIS vs. HAM		
				Total	Fine	Coarse
Total	Correlation coefficient (R)	0.85	0.69	0.70	0.62	0.42
	Slope	0.82±0.08	0.36±0.06	0.38±0.06	0.37±0.08	0.17±0.06
	Root mean square error (RMSE)	0.09	0.16	0.15	0.09	0.09
	Mean bias (MB)	−0.01	−0.10	−0.09	−0.04	−0.05
Bay of Bengal	Correlation coefficient (R)	0.92	0.68	0.75	0.65	0.24
	Slope	0.89±0.08	0.29±0.07	0.33±0.06	0.29±0.07	0.09±0.08
	Root mean square error (RMSE)	0.07	0.19	0.17	0.11	0.09
	Mean bias (MB)	−0.03	−0.15	−0.12	−0.07	−0.05
Arabian Sea	Correlation coefficient (R)	0.77	0.88	0.77	0.79	0.58
	Slope	0.76±0.16	0.55±0.08	0.49±0.1	0.68±0.14	0.22±0.08
	Root mean square error (RMSE)	0.11	0.10	0.11	0.05	0.09
	Mean bias (MB)	0.01	−0.04	−0.05	−0.01	−0.05

Discussion Paper | Discussion Paper | Discussion Paper | Discussion Paper |

ACPD

11, 13911–13946, 2011

Examination of aerosol distributions and radiative effects

R. Cherian et al.

Table 2. The direct aerosol radiative forcing (DARF, $W\,m^{-2}$) at the top of the atmosphere (TOA), at the surface (SUR), and within the atmosphere (ATM), and the atmospheric heating rate (K/day) over the Bay of Bengal and Arabian Sea legs during ICARB.

Region	HAM DARF ($W\,m^{-2}$)			Sunphotometer tied DARF ($W\,m^{-2}$)			Satellite tied DARF ($W\,m^{-2}$)			ICARB DARF ($W\,m^{-2}$) from Kedia et al. (2010)			Heating rate (K/day)
	TOA	SUR	ATM	TOA	SUR	ATM	TOA	SUR	ATM	TOA	SUR	ATM	
Total	−5.5	−12.1	6.6	−8.7	−19.9	11.1	−7.8	−17.8	9.9				0.26
Bay of Bengal	−5	−12.6	7.6	−9.8	−24.3	14.5	−8.6	−21.4	12.9	−12	−22.4	10.4	0.3
Arabian Sea	−6.2	−11.5	5.4	−7.4	−13.9	6.6	−6.8	−12.8	6	−10.5	−15.8	5.3	0.17

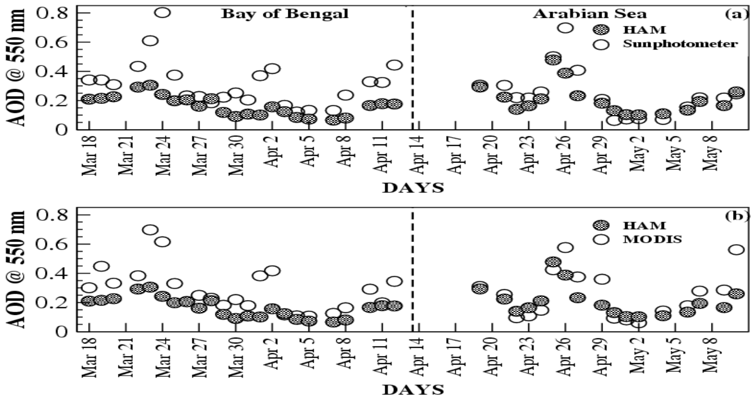

Fig. 1. Comparison of model derived aerosol optical depth (AOD) at 550 nm with **(a)** MODIS satellite retrievals and **(b)** ship-based remote sensing measurements during the ICARB cruise period from 18 March to 10 May 2006. See text for details.

ACPD
11, 13911–13946, 2011

Examination of aerosol distributions and radiative effects

R. Cherian et al.

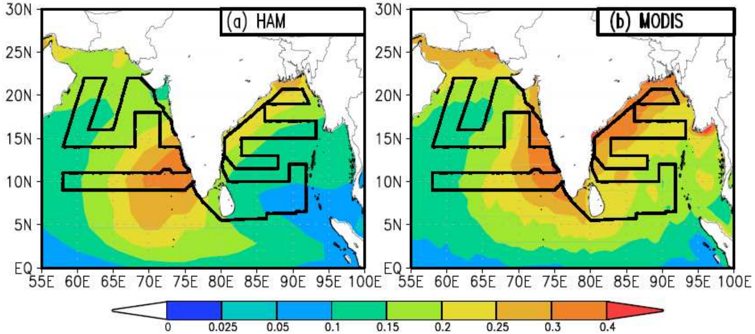

Fig. 2. AOD distributions at 550 nm wavelength **(a)** as simulated by ECHAM5.5-HAM and **(b)** as retrieved by the MODIS satellite sensors (Terra and Aqua combined), averaged over the ICARB cruise period.

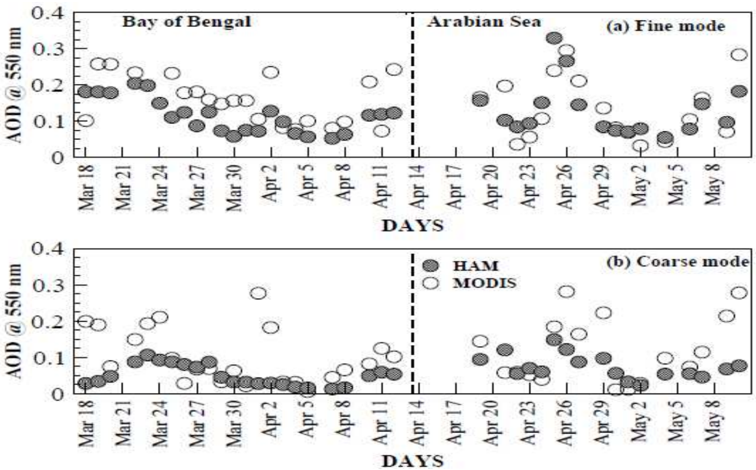

Fig. 3. Comparison of modelled fine (**a**; upper panel) and coarse mode (**b**; lower panel) AODs at 550 nm against satellite observations during the ICARB 2006 cruise period.

ACPD
11, 13911–13946, 2011

Examination of aerosol distributions and radiative effects

R. Cherian et al.

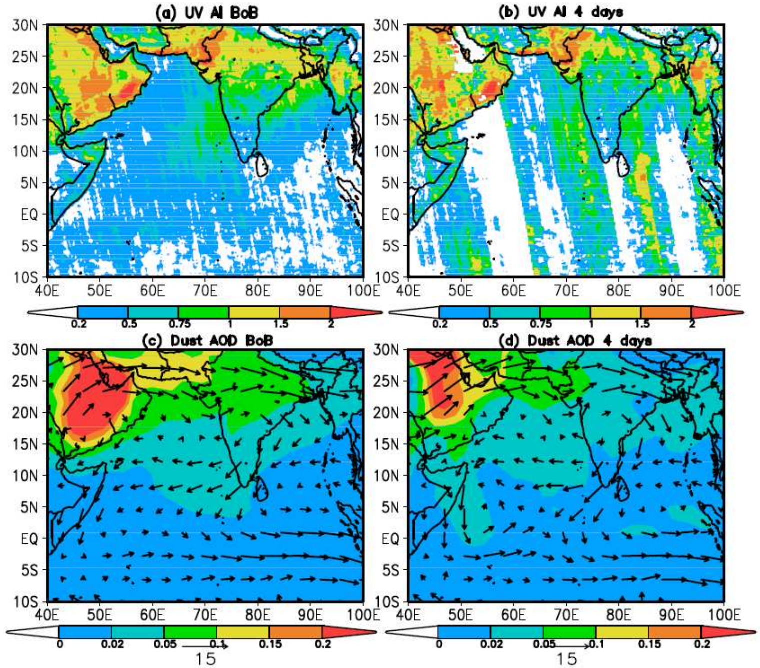

Fig. 4. Comparison of modelled dust AOD at 550 nm to Aura-OMI satellite derived UV Aerosol Index (AI) for the entire BoB periods (18 March–11 April; **a** and **c**) and for the average of 4 days where ECHAM5.5-HAM failed to capture large values of coarse-mode AOD (18 and 19 March, 1 and 2 April, **b** and **d**).

ACPD
11, 13911–13946, 2011

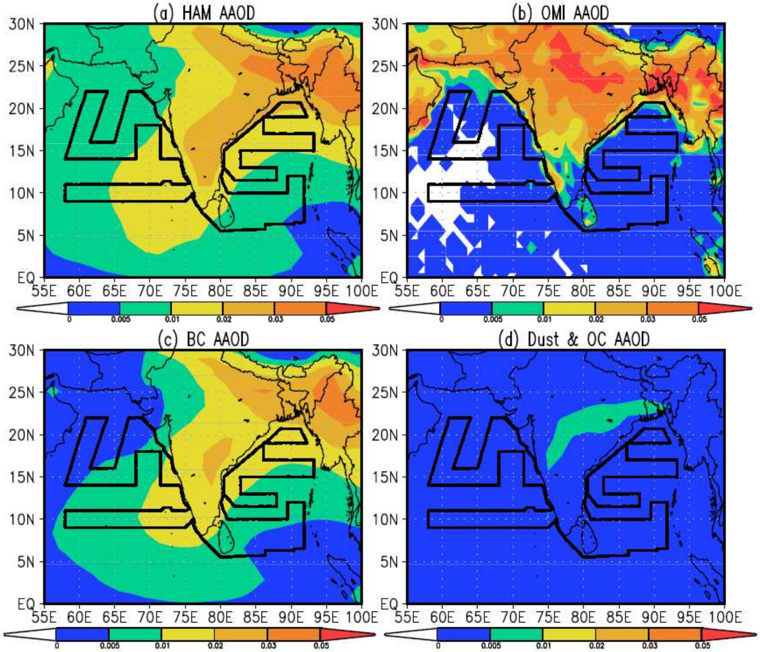

Fig. 5. Comparison of **(a)** modelled absorption optical depth (AAOD) at 550 nm and **(b)** Aura-OMI satellite derived AAOD at 500 nm averaged over the ICARB 2006 period. The simulated contributions of **(c)** BC and **(d)** Dust plus OC, to total AAOD, respectively, are also shown.

ACPD
11, 13911–13946, 2011

Examination of aerosol distributions and radiative effects

R. Cherian et al.

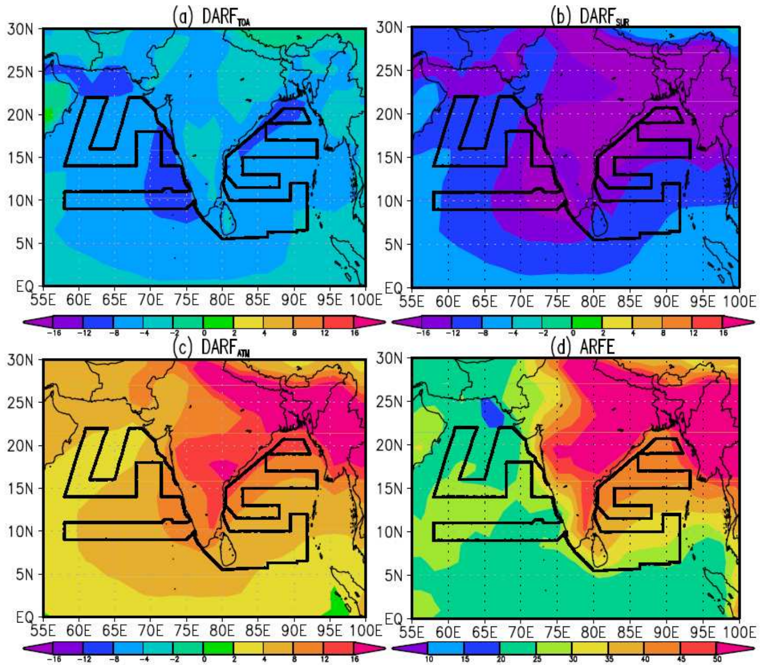

Fig. 6. Spatial distribution of clear-sky shortwave (SW) DARF (W/m^2) at the **(a)** top of the atmosphere (TOA), **(b)** surface (SUR), **(c)** within the atmosphere (ATM) and **(d)** atmospheric forcing efficiency (ARFE, $W\,m^{-2}\,\tau^{-1}$).

ACPD
11, 13911–13946, 2011

Examination of aerosol distributions and radiative effects

R. Cherian et al.

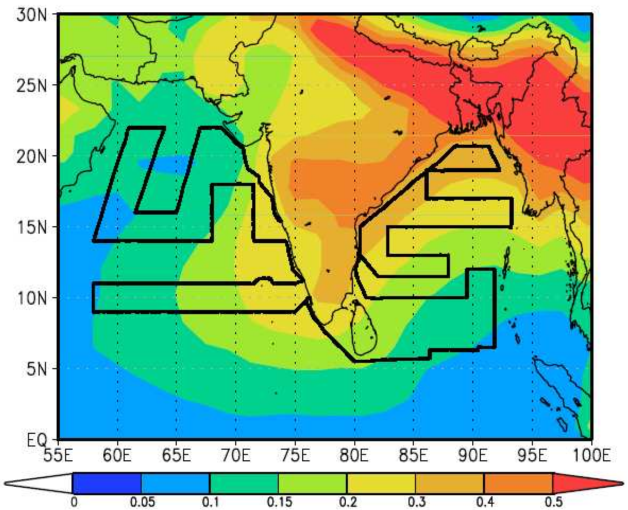

Fig. 7. Spatial distribution of mean solar heating rate (K day^{-1}) during ICARB 2006 period.

ACPD
11, 13911–13946, 2011

Examination of aerosol distributions and radiative effects

R. Cherian et al.